ACS APPLIED MATERIALS & INTERFACES

Research Article

www.acsami.org

Liquid Crystalline Perylene Diimide Outperforming Nonliquid Crystalline Counterpart: Higher Power Conversion Efficiencies (PCEs) in Bulk Heterojunction (BHJ) Cells and Higher Electron Mobility in Space Charge Limited Current (SCLC) Devices

Youdi Zhang,[†] Helin Wang,[†] Yi Xiao,*[,†] Ligang Wang,[‡] Dequan Shi,[‡] and Chuanhui Cheng*[,‡]

[†]State Key Laboratory of Fine Chemicals, Dalian University of Technology, Dalian 116024, People's Republic of China

[‡]School of Physical and Optoelectronic Engineering, Dalian University of Technology, Dalian 116024, People's Republic of China

Supporting Information

ABSTRACT: In this work, we propose the application of liquid crystalline acceptors as a potential means to improve the performances of bulk heterojunction (BHJ) organic solar cells. LC-1, a structurally-simple perylene diimide (PDI), has been adopted as a model for thorough investigation. It exhibits a broad temperature range of liquid crystalline (LC) phase from 41 °C to 158 °C, and its LC properties have been characterized by differential scanning calorimetry (DSC), polarization optical microscopy (POM), and X-ray diffraction (XRD). The BHJ devices, using P3HT:LC-1 (1:2) as an organic photovoltaic active layer undergoing thermal annealing at 120 °C, shows an optimized efficiency of 0.94 %. By contrast, the devices based on PDI-1, a nonliquid crystalline PDI counterpart, only obtain a much lower efficiency of 0.22%. Atomic force microscopy (AFM) images confirm that the active layers composed of P3HT:LC-1 have smooth and ordered morphology. In space charge limited current (SCLC) devices fabricated via a spin-coating technique, LC-1 shows the intrinsic electron mobility of 2.85×10^{-4} $cm^2/(V\ s)$ (at 0.3 MV/cm) which is almost 5 times that of PDI-1 (5.83×10^{-5} $cm^2/(V\ s)$) under the same conditions for thermal annealing at 120 °C.

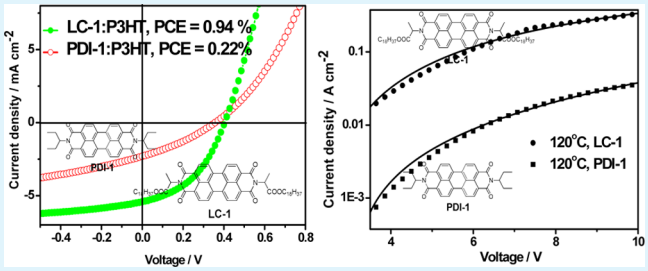

KEYWORDS: *bulk heterojunction solar cells, n-type semiconductor, perylene diimides, liquid crystalline, space charge limited current*

1. INTRODUCTION

In recent years, liquid crystalline (LC) semiconductors have received considerable attention in the fields of organic electronics.[1−4] Not only because they are readily dissolvable, but also because they self-assemble into highly ordered morphology[5] to effectively eliminate the structural and electronic defects.[6,7] LC materials are highly desirable for solution-processable devices.[8] It is not surprising that some space charge limited current (SCLC) devices and organic field-effect transistors (OFET) devices based on LC semiconductors have shown very high charge mobility.[9−13]

However, in the field of bulk heterojunction (BHJ) organic solar cells, the applicability of LC materials have not been well-recognized.[14] Actually, amorphous fullerenes derivatives, e.g., PCBM, firmly occupy the dominant status as electron acceptors in BHJ cells, although have poor absorption in solar spectrum. Generally speaking, there is still a wide gap between non-fullerene organic acceptors and fullerenes in terms of BHJ efficiency. Among all the reported nonfullerene acceptors, one representative class is perylene diimides (PDIs), which have very strong absorption in the visible region and exhibit high electron mobility. However, because of their large, rigid, and planar conjugation cores, the serious $\pi-\pi$ stacking and poor solubility of the PDIs and their analogues are problematic for BHJ cells; they tend to aggregate excessively to form islets, which not only damages the morphology of the BHJ active films but also generates carrier traps. A variety of strategies have been put forward to reduce the extent of $\pi-\pi$ stacking, improve solubility, and control the aggregation state.[15] These working concepts include the introduction of swallow tail-type long, branchy, and flexible alkyl side chains onto the two imide sites,[16−18] copolymerization of PDI and other conjugated monomer on the perylene bay sites,[19] direct connection of two PDI segments on the imide site to form nonplanar and nonconjugate dimers,[20] and combination of PDI and donor on the imide site to form co-oligomers,[21] etc.

Herein, we propose the utilization of liquid crystalline PDI derivatives, e.g., LC-1, as a new means parallel to the above-mentioned ones helping to improve the applicability of PDIs in BHJ cells. In this work, LC-1, which is a structurely simple PDI derivative acting as the model of our strategy, has been adopted as the acceptor in the fabrication of BHJ cells' active layers with P3HT as the donor. Devices based on LC-1 exhibit remarkably higher conversion efficiency than the nonliquid crystalline counterpart PDI-1.[15] To better understand the reason why

Received: August 9, 2013
Accepted: October 15, 2013
Published: October 15, 2013

LC-1 is in favor of BHJ solar cells, its LC properities have been thoroughly characterized by differential scanning calorimetry (DSC), polarization optical microscopy (POM), and X-ray diffraction (XRD); In addition, in spin-coated SCLC devices, LC-1's intrinsic electron mobility is much higher than that of PDI-1.

2. RESULTS AND DISCUSSION

2.1. Fundamental Characteristics of LC-1 Material. LC-1 molecule was designed and synthesized according to a previous procedure,[22] as shown in Scheme 1. Solubility of LC-1

Scheme 1. Synthetic Routes of the Investigated LC-1 Molecule

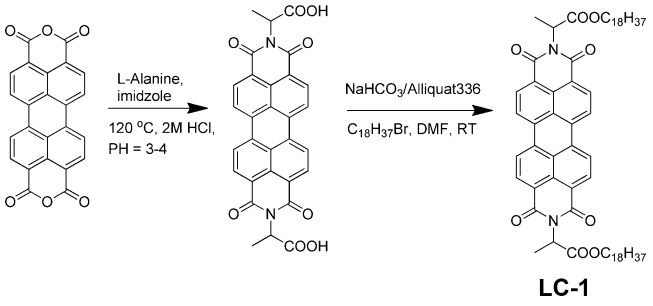

was 40 mg/mL in the common organic solution, e.g., dichloromethane, chloroform, chlorobenzene, and dichlorobenzene, and it was very important for applied in BHJ solar cells. IN addition, the absorption spectra of LC-1 do not have to change for modification of PDI N-terminal chains at 527 nm in the solution and at 495 nm in the film (see Figure 1). The

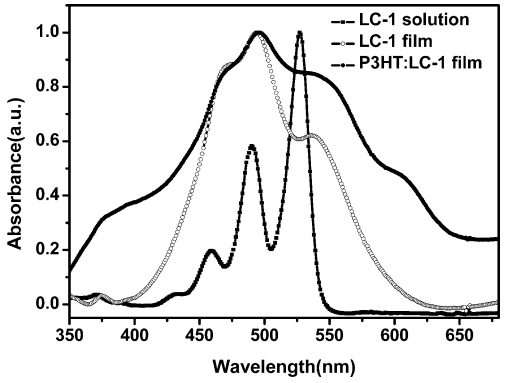

Figure 1. Normalized absorption spectra of (■) LC-1 chloroform solution (1×10^{-5}), (○) LC-1 film, and (●) P3HT:LC-1 blended film.

thermogravimetric analysis (TGA) curve showed the enhanced thermal stability for LC-1 with a decomposition onset temperature (T_d) of ~333.7 °C (see Figure 2).

2.2. Photovoltaic Device Performance. In the comparison investigation on BHJ devices using liquid crystalline LC-1 and n PDI-1, respectively, as acceptor materials, cells based on LC-1 exhibited remarkably superior performances. For the device with P3HT:LC-1 as an photovoltaic active layer, the optimum power conversion efficiency (PCE) was 0.94%, which is ~4 times that of a device based on the P3HT:PDI-1 (maximum PCE of 0.22%). These data supported our hypothesis that liquid crystalline acceptor materials are more advantageous in BHJ solar cells.

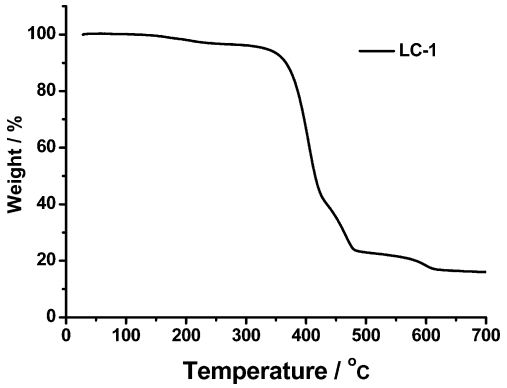

Figure 2. TGA thermograms of liquid crystalline molecule LC-1 measured under nitrogen flow (50 mL min^{-1}) at a heating rate of 10 °C min^{-1}.

Interestingly, there exists the regularity in the high dependence of devices's performances on the annealing temperature, which is related to the broad temperature range of LC-1's liquid crystalline phase. Keeping the P3HT:LC-1 weight ratio fixed at 1:2 in the active layer, and setting a series annealing temperature (50, 80, 100, 120, 150, and 165 °C), we tested the $J-V$ curves of a group of BHJ devices (100 mW cm^{-2} AM 1.5G), as recorded in Figure 3, and we summarized the corresponding data in Table 1.

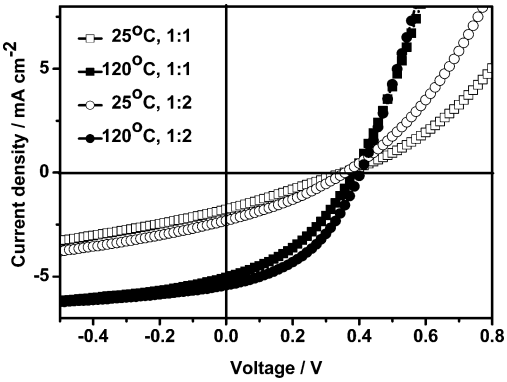

Figure 3. Current–voltage ($J-V$) curves of photovoltaic devices using P3HT:LC-1 as active layers at temperatures of 25 and 120 °C and weight ratios of 1:1 and 1:2, respectively. The curves correspond to the curve of P3HT:LC-1 using (□) a weight ratio of 1:1 at 25 °C, (■) a weight ratio of 1:1 at 120 °C, (○) a weight ratio of 1:2 at 25 °C, and (●) a weight ratio of 1:2 at 120 °C.

Particularly, the correlation between annealing temperature and PCE and the correlation between annealing temperature and short-circuit current (J_{SC}) had been clearly demonstrated in Figure 4. With the increase in annealing temperature from 50 °C to 120 °C, the continuous and obvious enhancements in device parameters including J_{SC}, open-circuit voltage (V_{OC}), and fill factor (FF) were found. The increased J_{SC} may result from a reorientation and enhanced ordering of the LC-1 during annealing, which would facilitate charge transport. However, at >120 °C, further increases in the annealing temperature induced a decrease in device performance. Thus, using thermal annealing at 120 °C resulted in the best data: PCE = 0.94%, V_{OC} = 0.41 V, J_{SC} = 5.42 mA cm^{-2}, and FF = 0.42. In the control experiment, the BHJ device unannealed at 25 °C only showed a much lower PCE of 0.23%, which is only a quarter of the optimum efficiency. When we changed the P3HT:LC-1 blended ratio into 1:1, the similar regularity on the effects of annealing temperature to

Table 1. Performance of the Devices with Different Weight Ratios and Thermal Annealing Conditions of P3HT:LC-1 from *o*-Dichlorobenzene Solution Used for Spin Coating

temperature [°C]	PCE [%]	J_{SC} [mA cm^{-2}]	V_{OC} [V]	FF
P3HT:LC-1 Weight Ratio = 1:1				
25	0.16	1.77	0.35	0.26
50	0.43	3.58	0.36	0.33
80	0.55	4.25	0.36	0.36
100	0.65	4.33	0.40	0.38
120	0.74	5.03	0.38	0.39
150	0.67	4.31	0.41	0.38
165	0.50	3.20	0.39	0.40
P3HT:LC-1 Weight Ratio = 1:2				
25	0.23	1.88	0.36	0.34
50	0.64	4.16	0.38	0.40
80	0.71	4.67	0.37	0.41
100	0.86	4.89	0.40	0.44
120	0.94	5.42	0.41	0.42
150	0.77	4.65	0.44	0.38
P3HT:PDI-1 Weight Ratio = 1:1[a]				
165	0.61	4.22	0.39	0.37
120	0.22	1.60	0.34	0.40

[a]The mixing solution of P3HT:PDI-1 was used as an organic photovoltaic active layer.

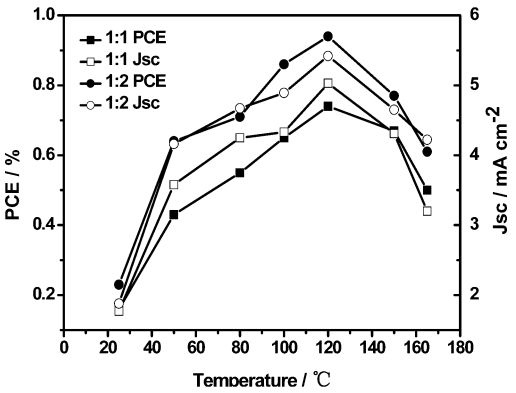

Figure 4. Relationship chart of PCE and J_{SC} versus temperature to P3HT:LC-1 at different temperatures and weight ratios.

device data had also been observed; Again, the best performance (PCE = 0.74%, V_{OC} = 0.38 V, J_{SC} = 5.03 mA cm^{-2}, and FF of 0.39) was obtained under the condition of thermal annealing at 120 °C.

However, in the BHJ devices using the nonliquid crystalline PDI-1 as the acceptor, thermal annealing did not seem to be as beneficial as it did to LC-1. After annealing at 120 °C, a device of P3HT:PDI-1 (1:1) showed a J_{SC} value of 1.6 mA cm^{-2}, V_{OC} = 0.34 V, FF = 0.40, and an efficiency of 0.22%. These data were much lower than those obtained from the P3HT:LC-1 device annealing at 120 °C, but were similar to those of the unannealed P3HT:LC-1 device. The above facts indicated that the improvement induced by thermal annealing was more related to LC-1's liquid crystalline feature than to the perylene diimide conjugation core.

To better understand the effects of the P3HT:LC-1 weight ratio to photovoltaic performances, the comparisons of different parameters (e.g., external quantum efficiencies (EQE) and internal quantum efficiencies (IQE)) were carried out. As shown in Figure 5A, the highest EQE (~17%) was obtained for the blends of 1:2 at 490 nm, while for P3HT:LC-1 (1:1) devices, the highest EQE value is just ~13% at 485 nm, the tested result implied that the increased proportion of LC-1 molecule produced more photocurrent in the blended films and also verified the improved J_{SC} observed in LC-1 devices, which showed higher EQE values (peak EQE = 17%) over the entire range of the active layer absorption from 350 nm to 700 nm, a significant portion of that photocurrent is due to absorption by the acceptor phase, followed by hole transfer to the donor. As shown in Figure 5B, the IQE tests also suggested that much more charge carriers were generated for P3HT:LC-1 (1:2) (~22%) under sunlight, compared with that of the doping ratio of 1:1 (~16%).

2.3. Atomic Force Microscopy Images. Atomic force microscopy (AFM) images revealed that the active layer morphology of P3HT:LC-1 were greatly influenced by their weight ratios and the thermal annealing. As shown in Figure 6, a P3HT:LC-1 ratio of 1:2 produced much smoother morphology than ratio of 1:1; Also, the morphology after thermal annealing at 120 °C was much smoother than that unannealed at 25 °C. The root-mean-square (RMS) surface roughness values could be the indicators for the quality of films: the smaller the RMS surface roughness, the better the film morphology. On one hand, the smallest RMS surface roughness of 4.67 nm for a doping ratio of 1:2 under the thermal annealing at 120 °C had been determined; this value was smaller than 5.50 nm, which corresponds to the film without annealing. On the other hand, for the unannealed film with a doping ratio of 1:1, the RMS surface roughness value was 7.61 nm, but after annealing at 120 °C, the value decreased to

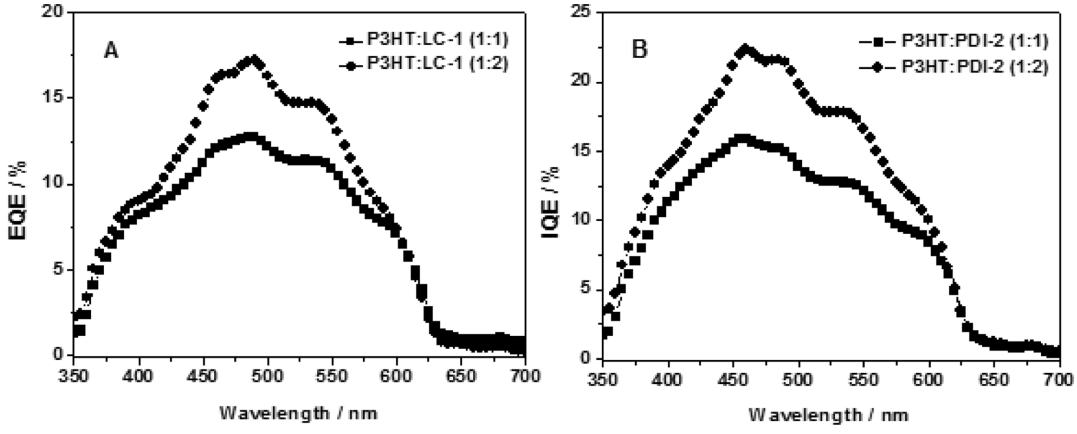

Figure 5. (A) External quantum efficiencies (EQE) and (B) internal quantum efficiencies (IQE) of P3HT:LC-1 at different weight ratios.

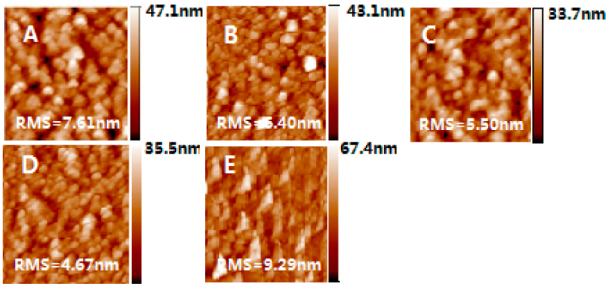

Figure 6. AFM height images (5 μm × 5 μm) of blended thin films of P3HT:LC-1 before thermal annealing (A) at 25 °C, P3HT:LC-1 = 1:1; (B) at 120 °C, P3HT:LC-1 = 1:1; (C) at 25 °C, P3HT:LC-1 = 1:2) and after thermal annealing ((D) at 120 °C, P3HT:LC-1 = 1:2; and (E) at 120 °C, P3HT:PDI-1 = 1:1).

6.40 nm. The decrease in the roughness of the blend films after annealing was due to the fact that the LC-1 molecules were self-organized into ordered structures at 120 °C within the liquid crystalline phase. The phenomenon that the increase in the proportion of LC-1 in the blended film can improve morphology should also be ascribed to liquid crystalline characteristics. Because of the nonliquid crystalline feature of PDI-1, the morphology of the P3HT:PDI-1 films would not be improved by the thermal annealing; the RMS surface roughness was high, up to 9.29 nm, even after annealing at 120 °C. Since the smooth morphology leaded to an efficient charge separation, higher J_{SC} and PCE for BHJ PV devices based on the thermally annealed blend films of P3HT:LC-1 than those of P3HT:PDI-1 can be partially explained.

2.4. Charge Mobility. Charge mobility within an active layer film is another critical factor for BHJ cells. Since we had already found that, in P3HT:LC-1 BHJ devices, thermal annealing greatly improved the PCE, for the sake of deeper interpretation of such effect, it would be useful to evaluate LC-1's electron mobility at different annealing temperature. Hence, we adopted the space charge limited current (SCLC) method,[12,23−26] which is suitable for determining organic semiconductors' intrinsic carrier mobility under steady-state current. Consistent with the former P3HT:LC-1 bulk heterojunction solar cells device structure, the SCLC devices' structure was designed to be ITO/ZnO (~30 nm)/LC-1 (~250 nm)/LiF (1.5 nm)/Al (100 nm). $J-V$ curves of the SCLC devices with spin-coated LC-1 as the active layer annealed at different temperatures were recorded (Figure 7), and the corresponding

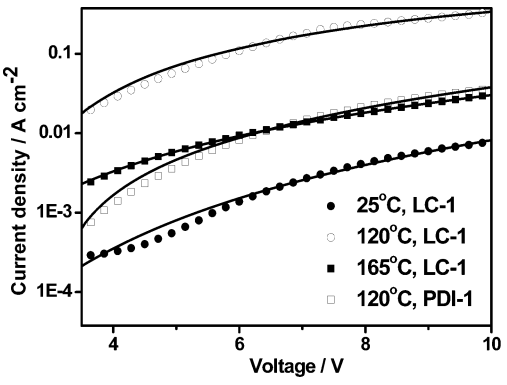

Figure 7. Current density versus voltage ($J-V$) characteristics of an electron-only device based on (●) LC-1 at 25 °C, (○) LC-1 at 120 °C, (■) LC-1 at 165 °C, and (□) PDI-1 at 120 °C at an electric field strength of 0.3 MV/cm.

Table 2. Performance of the Single Electron Devices LC-1 with Different Thermal Annealing Conditions from Chloroform Solution Used for Spin Coating at an Electric Field of 0.3 MV/cm

temperature [°C]	μ [cm^2/(V s)]	μ_0 [cm^2/(V s)]	γ [cm/V]
	LC-1		
25	4.90×10^{-6}	1.16×10^{-7}	0.0068
50	1.72×10^{-5}	7.81×10^{-6}	0.0014
80	2.91×10^{-5}	1.05×10^{-5}	0.0018
100	3.92×10^{-5}	1.02×10^{-6}	0.0066
120	2.85×10^{-4}	1.92×10^{-5}	0.0049
150	2.93×10^{-5}	3.95×10^{-7}	0.0078
165	1.74×10^{-5}	5.37×10^{-6}	0.0021
	PDI-1[a]		
120	5.83×10^{-5}	4.35×10^{-7}	0.0089

[a]The single electron device based on PDI-1 from chloroform solution used for spin coating at an electric field of 0.3 MV/cm.

parameters have been collected in Table 2. The SCLC in this case of mobility, depending on the field, can be approximated by the following formula:[27,28]

$$J = \frac{9}{8}\varepsilon\varepsilon_0\frac{E^2}{L}\mu_0 \exp(0.89\gamma\sqrt{E})$$

where E is the electric field across the sample; ε and ε_0 are the relative dielectric constant and the permittivity of the free space, respectively; and L is the thickness of the organic layer, with μ_0 the zero-field mobility and γ describing the field activation of the mobility.

With the increase in annealing temperature, the electron mobility of LC-1 first increased sharply, e.g., from 4.90×10^{-6} cm^2/(V s) at 25 °C to 1.72×10^{-5} cm^2/(V s) (at 0.3 MV/cm) at 50 °C; such a tendency of increase ceased at 120 °C, where the electron mobility achieved the highest value, 2.85×10^{-4} cm^2/(V s), which is 50 times higher than that of the unannealed device (25 °C); Then, further temperature elevation would result in an apparent decrease in electron mobility, e.g., to 2.93×10^{-5} cm^2/(V s) at 150 °C. Amazingly, such a correlation between the electron mobility of LC-1 and annealing temperature exhibited the same regularity as that of the PCE of P3HT:LC-1 BHJ solar cells. Hence, the best PCE of BHJ solar cells at 120 °C can be reasoned by the highest electron mobility of LC-1 at this temperature.[29,30]

The SCLC device using the nonliquid crystalline PDI-1 had also been tested. However, even if PDI-1 film had undergone the thermal annealing at 120 °C, the SCLC electron mobility was determined to be 5.83×10^{-5} cm^2/(V s), which is only one quarter of that of LC-1. This fact could be used to explain why BHJ cells using LC-1 as an acceptor outperformed those using PDI-1.

In BHJ organic solar cells, the balanced charge carrier mobilities reveal that LC-1 increases the FF and PCE, because of charge separation.[31,32] To investigate the carrier mobilities (electron and hole) in the blend films, the $J-V$ characteristics of the hole-only (ITO/PEDOT:PSS/LC-1 or PDI-1:P3HT/Au structure) and electron-only (Al/LC-1 or PDI-1:P3HT/LiF/Al structure) devices were measured for the as-cast and annealed blended films (see Tables 3 and 4). The hole and electron mobilities were extracted using the SCLC model[33,34] (Figure 8). For the annealed blended film at 120 °C, the values of the hole and electron mobilities are ~1.07×10^{-6} and ~1.28×10^{-5} cm^2/(V s), respectively. However, the hole and electron mobilities for the

as-cast blend are ~1.07 × 10^{-7} and 8.20 × 10^{-8} $cm^2/(V\ s)$, respectively. As the annealing temperature increases up to 120 °C, the hole mobility and electron mobility increase, which can be attributed to the improvement of film morphology and, thereby, is the reason for the higher PCE. However, the hole mobility and electron mobility of the PDI-1:P3HT film are 5.52 × 10^{-5} and 4.58 × 10^{-7} $cm^2/(V\ s)$ at 120 °C, respectively. Obviously, the strong aggregation tendency of nonliquid crystalline PDI-1 can result in more charge recombination and unbalanced charge transport in the blend films, which explains the lower performance of PDI-1:P3HT BHJ devices.

Since the investigations of all of the above devices had indicated that the annealing temperature played a decisive role in improving the PCE, mobility, and morphology, thoroughly investigating the thermal properties of LC-1 should be carried out to provide deeper insight into the correlation between the liquid crystalline phase and the suitable annealing temperature.

Table 3. Electron Mobilities of LC-1:P3HT with Different Thermal Annealing Condition and the Blended Film of 2:1 from *o*-Dichlorobenzene Solution Used for Spin Coating at an Electric Field of 0.3 MV/cm

temperature [°C]	μ_e [$cm^2/(V\ s)$]	μ_0 [$cm^2/(V\ s)$]	γ [cm/V]
	LC-1:P3HT		
25	8.20 × 10^{-8}	7.76 × 10^{-9}	0.0043
50	2.33 × 10^{-6}	1.24 × 10^{-7}	0.0053
80	3.33 × 10^{-6}	1.36 × 10^{-7}	0.0058
100	9.42 × 10^{-6}	4.43 × 10^{-7}	0.0056
120	1.28 × 10^{-5}	1.44 × 10^{-6}	0.0040
150	3.34 × 10^{-6}	3.10 × 10^{-8}	0.0085
165	1.96 × 10^{-7}	2.33 × 10^{-8}	0.0081
	PDI-1:P3HT[a]		
120	4.58 × 10^{-7}	3.89 × 10^{-9}	0.0087

[a]The electron mobility based on PDI-1:P3HT blended film from *o*-dichlorobenzene solution used for spin coating at an electric field of 0.3 MV/cm.

Table 4. Hole Mobilities of LC-1:P3HT with Different Thermal Annealing Condition and the Blended Film of 2:1 from *o*-Dichlorobenzene Solution Used for Spin Coating at an Electric Field of 0.3 MV/cm

temperature [°C]	μ_h [$cm^2/(V\ s)$]	μ_0 [$cm^2/(V\ s)$]	γ [cm/V]
	LC-1:P3HT		
25	1.07 × 10^{-7}	9.32 × 10^{-9}	0.0044
50	2.70 × 10^{-7}	4.02 × 10^{-8}	0.0035
80	3.97 × 10^{-7}	4.94 × 10^{-8}	0.0039
100	9.12 × 10^{-7}	4.85 × 10^{-7}	0.0011
120	1.07 × 10^{-6}	2.21 × 10^{-7}	0.0029
150	5.83 × 10^{-7}	2.49 × 10^{-8}	0.0057
165	3.20 × 10^{-7}	5.08 × 10^{-8}	0.0033
	PDI-1:P3HT[a]		
120	5.52 × 10^{-5}	2.18 × 10^{-7}	0.0101

[a]The hole-only mobility based on PDI-1:P3HT blended film from *o*-dichlorobenzene solution used for spin coating at an electric field of 0.3 MV/cm.

Since the investigations of all of the above devices had indicated that the annealing temperature played a decisive role in improving the PCE, mobility, and morphology, thoroughly investigating the thermal properties of LC-1 should be carried out to provide deeper insight into the correlation between the liquid crystalline phase and the suitable annealing temperature.

2.5. Differential Scanning Calorimetry (DSC), Polarization Optical Microscopy (POM), and X-ray Diffraction (XRD). As shown in Figure 9, the DSC heating curve of LC-1 showed two reversible transitions: at 54 °C and 172 °C. The corresponding transitions upon cooling were observed at 158 °C and 41 °C. Such information indicated a broad liquid crystalline phase (~112 °C), which was conductive to optimizing the annealed temperature for organic photovoltaic devices. The P3HT:LC-1 BHJ devices that underwent annealing at 120 °C generated a highest PCE, possibly because this annealing temperature was in the upper section of the liquid crystalline phase.

POM (see Figure 10) experiments upon cooling from the isotropic melt gave evidence for a highly ordered mesophase which is a typical characteristics for the liquid crystalline materials.[22,35−37] Figure 10A at 120 °C showed that the entire glass substrate covered a very compact and uniform film composed of small snowflake-like textures, in contrast to Figure 10B at 165 °C with the larger and inhomogenous islets. The results implied that thermal annealing at different temperature would influence the particle size and uniformity in the mesophases to different extents and, thus, affect the electron mobility[38] and PCE. So, there was no wonder that annealing at

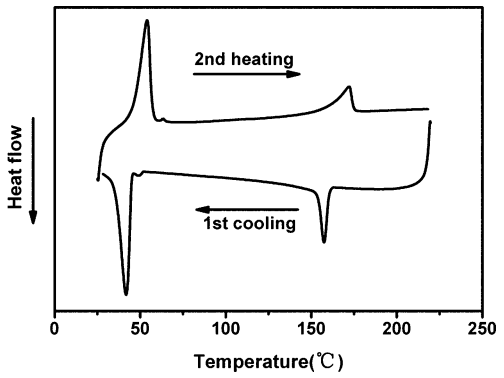

Figure 9. Differential scanning calorimetry (DSC) traces of LC-1 at a ramp rate of 10 °C/min.

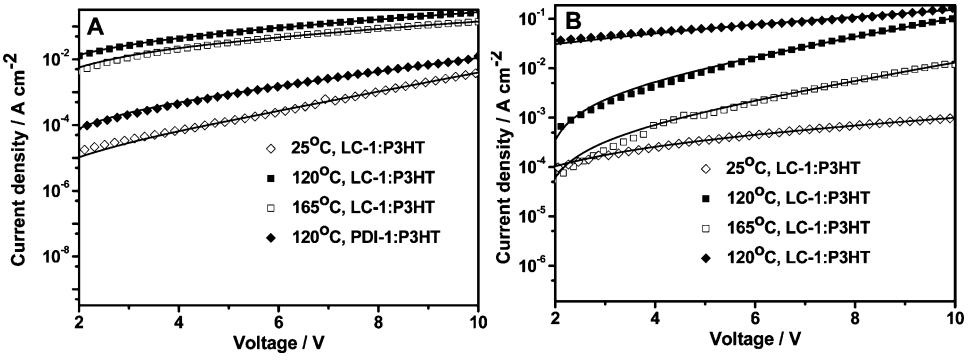

Figure 8. Current density versus voltage ($J-V$) characteristics of (A) electron-only devices and (B) hole-only devices based on (◇) LC-1:P3HT at 25 °C, (■) LC-1:P3HT at 120 °C, (□) LC-1:P3HT at 165 °C, and (◆) PDI-1 at an electric field strength of 0.3 MV/cm.

dx.doi.org/10.1021/am4033185 | ACS Appl. Mater. Interfaces 2013, 5, 11093−11100

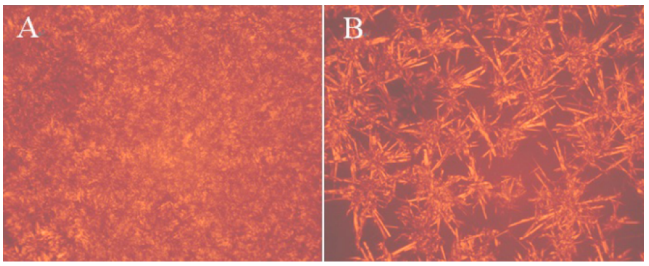

Figure 10. Polarizing optical microscopy (POM) images of LC-1 (under crossed polarizers) at (A) 120 °C and (B) 165 °C.

120 °C resulted in highest electron mobility of LC-1 and the best performance in BHJ solar cells.

Also, XRD experiments were in accordance with a columnar smectic ordering of the mesogens. The diffractogram of LC-1 from 25 °C to 165 °C are shown in Figure 11. The diffraction

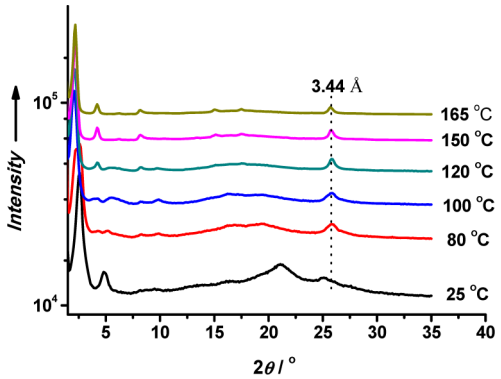

Figure 11. X-ray diffraction (XRD) patterns of LC-1 at 25, 80, 100, 120, 150, and 165 °C.

peaks of the 25 °C sqample showed a relatively weak and wide single peak at $2\theta = 2.55°$ (corresponding to 34.61 Å). However, upon further heating LC-1 into a liquid crystalline phase, a strong and narrow diffraction peak at $2\theta = 2.14°$ (41.23 Å) and $2\theta = 25.85°$ (3.44 Å) appeared and became more and more sharp as the temperature increased. The reflection at 25.85° in the wide-angle regime depicts a moderate intracolumnar long-range order with a $\pi-\pi$ stacking distance of $d_{\pi\pi} = 3.44$ Å. LC-1 crystalline at 165 °C was the best and was much better than that at 25 °C. Meanwhile, we found that, at higher temperature, the overall diffraction peaks move slightly toward the direction of the small-angle diffraction. While new diffraction peaks at $2\theta = 9.2°$, 15.1°, and 17.8° emerged at higher temperature, the original peak with $2\theta = 21.1°$ in the 25 °C diffractogram disappeared in the wide-angle regime. These changes reflected that, in the liquid crystalline phase, LC-1 has a highly ordered columnar smectic phase, which is similar to the results of Jin, who had studied a series of LC PDI derivatives containing amino-acids eater and found they have the parallel stacking forms in LC phase.

XRD diffraction patterns of the blended LC-1:P3HT (2:1) films reveal that thermal annealing is critical for the films' crystallinity, as shown in Figure 12. The best annealing temperature is 120 °C, which results in sharper and stronger peaks at $2\theta = 2.43°$ and 4.66° than other temperatures. Although these two 2θ peaks are the distinct packing characteristics of all the perylenediimides, they do not appear in the XRD patterns of the films annealed at lower

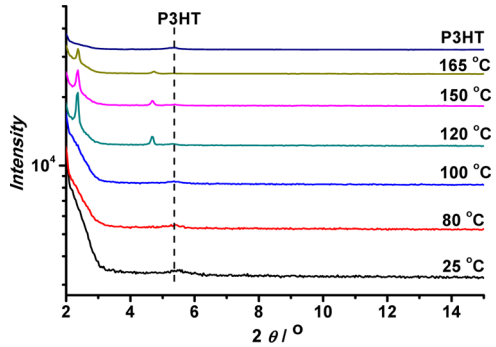

Figure 12. XRD patterns of LC-1:P3HT (2:1) blended films from *o*-dichlorobenzene solution used for spin coating on ITO/PEDOT:PSS substrate. In addition, the blend films are measured at room temperature (RT) without annealing and after annealing at 80, 100, 120, 150, and 165 °C.

temperatures (25, 80, and 100 °C). Thus, the side chains of LC-1 endue this PDI derivative a reasonable self-tunability in packing behavior. While P3HT shows only very weak and broad diffraction peaks, indicating quite disordered donor phases, the highly ordered arrangement in the blend film annealed at 120 °C can only be attributed to liquid crystalline phase of LC-1. The above XRD results of the blended films are identical to that of the pure LC-1, which again confirms that thermal annealing at a higher temperature within liquid crystalline phase will produce optimum PCE in BHJ organic solar cells.

3. CONCLUSION

In summary, we have developed and characterized a liquid crystalline perylene diimide acceptor LC-1. It exhibited a liquid crystalline phase with a broad temperature range from 41 °C to 158 °C, which is essential for optimizing the thermal annealing to improve the morphology of organic films, charge mobility, and device efficiency. The LC properties of LC-1 have been thoroughly investigated by DSC, POM, and XRD. During device investigation, it is found that 120 °C is the best temperature for thermal annealing, which results in the highest electron mobility in SCLC devices and highest PCE in BHJ solar cells. This temperature is in the upper part of the LC phase, at which LC-1 forms highly ordered films with compact and uniform crystalline particles. The BHJ devices, using P3HT:LC-1 (1:2) as organic photovoltaic active layer undergoing thermal annealing at 120 °C, shows an optimized efficiency of 0.94%. In contrast, the devices based on PDI-1, which is a nonliquid crystalline PDI counterpart, only obtain a much lower efficiency of 0.22%. Atomic force microscopy (AFM) images confirm that the active layers composed of P3HT:LC-1 have smooth and ordered morphology. In SCLC devices fabricated via the spin-coating technique, LC-1 shows the intrinsic electron mobility of 2.85×10^{-4} cm^2/(V s), which is almost 5 times that of the PDI-1 value (5.83×10^{-5} cm^2/(V s)) under the same conditions for thermal annealing at 120 °C. Because of the broad temperature range of the liquid crystalline phase of LC-1, thermal annealing at higher temperatures will result in mild aggregation and thus, improve the order and morphology of the LC-1:P3HT blended films, which is favorable for the balanced electron and hole transport and thereby higher PCE. However, when using nonliquid crystalline PDI-1 as an acceptor, its strong aggregation results in poor exciton dissociation and charge transport of the blend films.

Thus, LC-1 is more competent than PDI-1. This concept of utilizing liquid crystalline perylene diimide is worth extending to other types of non-fullerene organic semiconductors in order to discover more efficient alternatives to PCBM and further improve the performances of BHJ solar cells.

4. EXPERIMENTAL SECTION

Synthesis of LC-1. *N,N′*-di((S)-1-carboxylethyl)-3,4:9,10-perylenetetracarboxyldiimide and LC-1 was synthesized according to procedures reported by Jin's group.[22] *N,N′*-di((S)-1-carboxylethyl)-3,4:9,10-perylenetetracarboxyldiimide (6.95 g, 12.99 mmol) was dissolved in an aqueous solution of 5 % $NaHCO_3$(100 mL). ALIQUAT 336 (9.6 g, ca. 20 mmol) was dissolved in a 2:1 (v/v) ethanol/water mixture (120 mL). The two solutions were mixed and stirred at room temperature for 30 min. The mixture was then extracted three times with petroleum ether (500 mL), and the combined petroleum ether solution was evaporated to dryness. The residue was further dried at 75 °C for 2 h in a vacuum oven and then dissolved in dimethylformamide (DMF) (100 mL). 1-Bromooctadecane (9.54 g, 28.6 mmol) was added and the mixture was stirred at room temperature for 12 h. The mixture was then poured into methanol (400 mL). The product was collected as an orange powder via suction filtration and washed thoroughly with methanol. After drying, the product LC-1 at 75 °C in a vacuum oven to constant weight, it was purified by column chromatography on silica gel using 4:1 (v/v) CH_2Cl_2/*n*-hexane as the eluent. Yield: 10.50 g (78%). ^{1}H NMR (400 MHz, $CDCl_3$, δ) 8.58 (d, 2H), 8.43 (t, 2H), 5.79 (m, 1H), 4.29−4.10 (m, 2H), 1.82−1.54 (m, 5H), 1.19 (d, 30H), 0.87 (t, 3H); ^{13}C NMR (100 MHz, $CDCl_3$, δ) 170.44, 162.73, 134.69, 131.76, 129.47, 126.38, 123.22, 65.89, 49.77, 32.10, 29.86, 29.71, 29.54, 29.38, 28.66, 26.10, 22.87, 14.98, 14.30; HRMS (MALDI-TOF, m/z): [M +Na]+ calcd for $C_{66}H_{90}N_2O_8Na$, 1061.6595; found, 1061.6569. ^{1}H and^{13}C NMR spectra of the final product, LC-1, are provided in the Supporting Information.

Materials Characterization. ^{1}H and ^{13}C NMR spectra were recorded using a 400 MHz Bruker in $CDCl_3$ at 293 K using TMS as a reference. Accurate mass correction was measured with MALDI ToF mass spectrometer (MALDI micro MX). Thermogravimetric analysis (TGA) were carried out using a Mettler−Toledo TGA/SDTA 851e at a heating rate of 10 °C min^{-1} under nitrogen flow of 20 mL min^{-1}. Differential scanning calorimetry (DSC) analyses were performed on a DSC Q100 (TA Instruments). DSC curves were recorded at a scanning rate of 10 °C min^{-1} under nitrogen flow. Phase transitions were also examined using a POM Nikon Diaphot 300 with a Mettler FP 90 temperature-controlled hot stage. X-ray diffraction (XRD) measurements were performed on a Bruker D8 Avance equipped with a Huber quartz monochromator 611 with Cu Kα_1 = 1.54051 Å. Film thicknesses were determined on an Alphastep 500 surface profilometer. UV-vis absorption spectra in chloroform ($CHCl_3$) solution were recorded in a UV-vis spectrophotometer (Model HP8453) at room temperature using a glass cuvette with a path length of 1 cm.

Device Preparation and Characterization. BHJ organic device preparation proceeds as follows. A 15 Ω cm^{-2} resistor of indium-doped tin oxide (ITO) substrate was purchased from Xiangcheng Science and Technology Co., Ltd., and then the substrates underwent a cleaned course in an ultrasonic bath with acetone, ethanol, and ultrapure water and dried for 1 h under a blast dry oven. Subsequently, the glasses were cleaned in oxygen plasma treatment for 10 min, and a PEDOT:PSS (Clevios P VP AI 4083, H.C. Starck) solution was then spin-coated at 2000 rpm for 60 s onto the cleaned ITO surface, resulting in a thickness of ∼40 nm, as determined with a Dektak surface profilometer. The PEDOT:PSS layer was annealed for 30 min at 120 °C in air.

A solution of active layer P3HT (Rieke No. 4002-E) and LC-1 were simultaneously dissolved in dichlorobenzene in a weight ratio of 1:1 at a concentration of 15 mg mL^{-1} and stirred for 1 h at a temperature of 90 °C in an oil bath. Before deposition of the active layer, the mixed solution of P3HT:LC-1 was filtered through a polytetrafluoroethylene (PTFE) syringe filter (0.45 μm pore size). The active layer was then spin-coated on top of the PEDOT:PSS film at 600 rpm (dichlorobenzene) for 18 s resulting in a film thickness of ∼96 nm. Aluminum counter electrodes were evaporated through a shadow mask on top of the active layer with a thickness of ∼100 nm. The films were annealed at 120 °C for 30 min in the vacuum state. The active area of the pixels, as defined by the overlap of anode and cathode area, was 12 mm^2. The photovoltaic performance was determined under simulated sunlight, using a commercial solar simulator (Zolix ss150 solar simulator, China).

Device Characterization. The external quantum efficiency (EQE) characterization of all devices was performed in air. The light output from a xenon lamp was monochromated by a Digichrom Model 240 monochromator, and the short-circuit device photocurrent was monitored by a Keithley electrometer as the monochromator was scanned. A calibrated silicon photodiode (818-UV Newport) was used as a reference in order to determine the intensity of the light incident on the device, allowing the EQE spectrum to be deduced.

■ ASSOCIATED CONTENT

Ⓢ Supporting Information

^{1}H and ^{13}C NMR spectra of LC-1. Thermal gravimetric analysis (TGA) of LC-1. UV-vis absorption spectra of LC-1 in chloroform ($CHCl_3$) solution and the film. This material is available free of charge via the Internet at http://pubs.acs.org.

■ AUTHOR INFORMATION

Corresponding Authors

*E-mail: xiaoyi@dlut.edu.cn.

*E-mail: chengchuanhui@ dlut.edu.cn.

Author Contributions

The manuscript was written through contributions of all authors. All authors have given approval to the final version of the manuscript.

Notes

The authors declare no competing financial interest.

■ ACKNOWLEDGMENTS

This work was supported by National Natural Science Foundation of China (No. 21174022), National Basic Research Program of China (No. 2013CB733702) and Specialized Research Fund for the Doctoral Program of Higher Education (No. 20110041110009).

■ REFERENCES

(1) Li, Q., Ed. *Self-Organized Organic Semiconductors: From Materials to Device Applications*; John Wiley & Sons: Hoboken, NJ, 2011.

(2) Li, Q., Ed. *Liquid Crystals Beyond Displays: Chemistry, Physics, and Applications*; John Wiley & Sons: Hoboken, NJ, 2012.

(3) Li, L.; Kang, S. W.; Harden, J.; Sun, Q.; Zhou, X.; Dai, L.; Jakli, A.; Kumar, S.; Li, Q. *Liq. Cryst.* **2008**, *35*, 233−239.

(4) Zhou, X.; Kang, S.-W.; Kumar, S.; Li, Q. *Liq. Cryst.* **2009**, *3*, 269−274.

(5) Zhou, X.; Kang, S.-W.; Kumar, S.; Kulkarni, R. R.; Cheng, S. Z. D.; Li, Q. *Chem. Mater.* **2008**, *20*, 3551−3553.

(6) Fitzner, R.; Elschner, C.; Weil, M.; Uhrich, C.; Koerner, C.; Riede, M.; Leo, K.; Pfeiffer, M.; Reinold, E.; Mena-Osteritz, E.; Baeuerle, P. *Adv. Mater.* **2012**, *24*, 675−680.

(7) Schrader, M.; Fitzner, R.; Hein, M.; Elschner, C.; Baumeier, B.; Leo, K.; Riede, M.; Baeuerle, P.; Andrienko, D. *J. Am. Chem. Soc.* **2012**, *134*, 6052−6056.

(8) Sun, Q.; Dai, L.; Zhou, X.; Li, L.; Li, Q. *Appl. Phys. Lett.* **2007**, *91*, 253505/1−253505/3.

(9) Struijk, C. W.; Sieval, A. B.; Dakhorst, J. E. J.; van Dijk, M.; Kimkes, P.; Koehorst, R. B. M.; Donker, H.; Schaafsma, T. J.; Picken,

S. J.; van de Craats, A. M.; Warman, J. M.; Zuilhof, H.; Sudholter, E. J. R. *J. Am. Chem. Soc.* **2000**, *122*, 11057−11066.
(10) Wen, Y.; Liu, Y.; Di, C.-a.; Wang, Y.; Sun, X.; Guo, Y.; Zheng, J.; Wu, W.; Ye, S.; Yu, G. *Adv. Mater.* **2009**, *21*, 1631−1635.
(11) Treier, M.; Arlin, J. B.; Ruzieacute, C.; Geerts, Y. H.; Lemaur, V.; Cornil, J.; Samori, P. *J. Mater. Chem.* **2012**, *22*, 9509−9512.
(12) Schmidt, R.; Oh, J. H.; Sun, Y.-S.; Deppisch, M.; Krause, A.-M.; Radacki, K.; Braunschweig, H.; Köenemann, M.; Erk, P.; Bao, Z.; Wüerthner, F. *J. Am. Chem. Soc.* **2009**, *131*, 6215−6228.
(13) An, Z.; Yu, J.; Domercq, B.; Jones, S. C.; Barlow, S.; Kippelen, B.; Marder, S. R. *J. Mater. Chem.* **2009**, *19*, 6688−6698.
(14) Lin, Y.; Li, Y.; Zhan, X. *Chem. Soc. Rev.* **2012**, *41*, 4245−4272.
(15) Kamm, V.; Battagliarin, G.; Howard, I. A.; Pisula, W.; Mavrinskiy, A.; Li, C.; Müellen, K.; Laquai, F. *Adv. Energy. Mater.* **2011**, *1*, 297−302.
(16) Holcombe, T. W.; Norton, J. E.; Rivnay, J.; Woo, C. H.; Goris, L.; Piliego, C.; Griffini, G.; Sellinger, A.; Bredas, J.-L.; Salleo, A.; Frechet, J. M. J. *J. Am. Chem. Soc.* **2011**, *133*, 12106−12114.
(17) Rajaram, S.; Armstrong, P. B.; Kim, B. J.; Frechet, J. M. J. *Chem. Mater.* **2009**, *21*, 1775−1777.
(18) Shin, W.-S.; Jeong, H.-H.; Kim, M.-K.; Jin, S.-H.; Kim, M.-R.; Lee, J.-K.; Lee, J. W.; Gal, Y.-S. *J. Mater. Chem.* **2006**, *16*, 384−390.
(19) Erjun, Z.; Junzi, C.; Qingshuo, W.; Tajima, K.; Chunhe, Y.; Hashimoto, K. *Angew. Chem., Int. Ed.* **2011**, *50*, 2799−2803.
(20) Rajaram, S.; Shivanna, R.; Kandappa, S. K.; Narayan, K. S. *J. Phys. Chem. Lett.* **2012**, *3*, 2405−2408.
(21) Bu, L.; Guo, X.; Yu, B.; Qu, Y.; Xie, Z.; Yan, D.; Geng, Y.; Wang, F. *J. Am. Chem. Soc.* **2009**, *131*, 13242−13243.
(22) Xu, Y.; Leng, S.; Xue, C.; Sun, R.; Pan, J.; Ford, J.; Jin, S. *Angew. Chem., Int. Ed.* **2007**, *46*, 3896−3899.
(23) Kaafarani, B. R.; Kondo, T.; Yu, J. S.; Zhang, Q.; Dattilo, D.; Risko, C.; Jones, S. C.; Barlow, S.; Domercq, B.; Amy, F.; Kahn, A.; Bredas, J. L.; Kippelen, B.; Marder, S. R. *J. Am. Chem. Soc.* **2005**, *127*, 16358−16359.
(24) Woo, C. H.; Thompson, B. C.; Kim, B. J.; Toney, M. F.; Frechet, J. M. J. *J. Am. Chem. Soc.* **2008**, *130*, 16324−16329.
(25) Jian-Yang, C.; Domercq, B.; Jones, S. C.; Junsheng, Y.; Xiaohong, Z.; Zesheng, A.; Bishop, M.; Barlow, S.; Marder, S. R.; Kippelen, B. *J. Mater. Chem.* **2007**, *17*, 2642−2647.
(26) An, Z. S.; Yu, J. S.; Jones, S. C.; Barlow, S.; Yoo, S.; Domercq, B.; Prins, P.; Siebbeles, L. D. A.; Kippelen, B.; Marder, S. R. *Adv. Mater.* **2005**, *17*, 2580−2583.
(27) Murgatroyd, P. N. *J. Phys. D: Appl. Phys.* **1970**, *3*, 151−156.
(28) Malliaras, G. G.; Salem, J. R.; Brock, P. J.; Scott, C. *Phys. Rev. B* **1998**, *58*, 13411−13414.
(29) Woo, C. H.; Holcombe, T. W.; Unruh, D. A.; Sellinger, A.; Fréchet, J. M. J. *Chem. Mater.* **2010**, *22*, 1673−1679.
(30) Bloking, J. T.; Han, X.; Higgs, A. T.; Kastrop, J. P.; Pandey, L.; Norton, J. E.; Risko, C.; Chen, C. E.; Brédas, J.-L.; McGehee, M. D.; Sellinger, A. *Chem. Mater.* **2011**, *23*, 5484−5490.
(31) Peumans, P.; Forrest, S. R. *Chem. Phys. Lett.* **2004**, *398*, 27−31.
(32) Koster, L. J. A.; Mihailetchi, V. D.; Blom, P. W. M. *Appl. Phys. Lett.* **2006**, *88*, 052104/1−052104/3.
(33) Karl, N. *Synth. Met.* **2003**, *133-134*, 649−657.
(34) Mihailetchi, V. D.; Duren, J. K. J.; van Blom, P. W. M.; Hummelen, J. C.; Janssen, R. A. J.; Kroon, J. M.; Rispens, M. T.; Verhees, W. J. H.; Wienk, M. M. *Adv. Funct. Mater.* **2003**, *13*, 43−46.
(35) Pisula, W.; Kastler, M.; Wasserfallen, D.; Robertson, J. W. F.; Nolde, F.; Kohl, C.; Muellen, K. *Angew. Chem., Int. Ed.* **2006**, *45*, 819−823.
(36) Marcon, V.; Kirkpatrick, J.; Pisula, W.; Andrienko, D. *Phys. Status Solidi B* **2008**, *245*, 820−824.
(37) Wicklein, A.; Lang, A.; Muth, M.; Thelakkat, M. *J. Am. Chem. Soc.* **2009**, *131*, 14442−14453.
(38) An, Z.; Yu, J.; Jones, S. C.; Barlow, S.; Yoo, S.; Domercq, B.; Prins, P.; Siebbeles, L. D. A.; Kippelen, B.; Marder, S. R. *Adv. Mater.* **2005**, *17*, 2580−2583.